HHS Public Access

Author manuscript

Mol Psychiatry. Author manuscript; available in PMC 2019 October 26.

Published in final edited form as:

Mol Psychiatry. 2019 November ; 24(11): 1627–1640. doi:10.1038/s41380-019-0412-6.

Pten loss results in inappropriate excitatory connectivity

Patrick D. Skelton, B.S.[1], **Paul W. Frazel, B.S.**[1], **Daehoon Lee, Ph.D.**[2], **Hoonkyo Suh, Ph.D.**[2], **Bryan W. Luikart, Ph.D.**[1,*]

[1]Department of Molecular and Systems Biology; Dartmouth Geisel School of Medicine; Hanover, NH, 03755; United States of America

[2]Department of Neurosciences; Cleveland Clinic; Cleveland, Ohio, 44195; United States of America

Abstract

Pten mutations are associated with Autism Spectrum Disorder. Pten loss of function in neurons increases excitatory synaptic connectivity, contributing to an imbalance between excitation and inhibition. We aimed to determine whether Pten loss results in aberrant connectivity in neural circuits. We compared postnatally generated wild-type and Pten knockout granule neurons integrating into the dentate gyrus using a variety of methods to examine their connectivity. We found that postsynaptic Pten loss provides an advantage to dendritic spines in competition over a limited pool of presynaptic boutons. Retrograde monosynaptic tracing with rabies virus reveals that this results in synaptic contact with more presynaptic partners. Using independently excitable opsins to interrogate multiple inputs onto a single neuron, we found that excess connectivity is established indiscriminately from among glutamatergic afferents. Therefore, Pten loss results in inappropriate connectivity whereby neurons are coupled to a greater number of synaptic partners.

Introduction

Pten is a lipid and protein phosphatase implicated in cancer and Autism Spectrum Disorder. As a lipid phosphatase, it dephosphorylates PIP_3, directly antagonizing PI3K to act as a negative regulator of the downstream AKT and mTOR pathways (1). Mutations in Pten have been found in cases of Autism Spectrum Disorder (ASD), often comorbid with macrocephaly and epilepsy (2–5). Large exome sequencing studies have also confirmed germline Pten mutations in ASD (6–9).

*Correspondence: Bryan Luikart, Bryan.W.Luikart@Dartmouth.edu, 74 College St., Vail 604, Hanover, NH, 03755, Telephone: 603-650-1633, Fax: 603-650-1188.

Author Contributions

Conceptualization: P.D.S, H.S., and B.W.L.; Methodology: P.D.S., H.S., and B.W.L.; Investigation: P.D.S., P.W.F., D.L.; Writing—Original Draft: P.D.S.; Writing—Review and Editing: P.D.S., H.S., and B.W.L.; Supervision: H.S. and B.W.L.; Funding Acquisition: H.S. and B.W.L.

Declaration of Interests

The authors declare no competing interests.

Supplementary Information

Supplementary information is available at MP's website.

Animal models demonstrate a role for Pten in brain development. Pten knockout in brain (10) and specific to forebrain neurons (11, 12) induces brain overgrowth, cellular hypertrophy, and seizures. Mice with Pten loss or mutation also show behavioral phenotypes reminiscent of ASD, including altered social behavior, anxiety, impaired learning, and hyperactivity (11–14). Pten has been implicated in a broad array of neurodevelopmental processes, including cell proliferation (15, 16), differentiation (14, 16, 17), and survival (18).

In individual neurons, Pten regulates synaptic connectivity. Pten deficiency causes hypertrophy of the soma (10, 11, 17, 19) and dendritic arbor (11, 20–24) in a wide variety of brain regions, cell types, and experimental systems. Synaptic alterations include increased density of dendritic spines and recruitment of excitatory synaptic input (20, 22, 25). Pten loss in postnatally generated neurons in the dentate gyrus is sufficient to cause epilepsy (15, 26), underscoring the increased recruitment of excitatory input.

Here, we determine whether the increased synaptogenesis and connectivity that results from Pten loss leads to miswiring of neural circuits. We demonstrate that the increased number of excitatory synapses onto Pten knockout neurons is due to an enhanced ability to compete with surrounding neurons for a limited pool of synaptic boutons. This leads to synaptic coupling with an increased number of presynaptic partners and increased excitatory drive from multiple afferents. Our results demonstrate that the increased synaptic connectivity of Pten knockout neurons is dependent on the availability of presynaptic partners, and that it is not biased toward a specific population. Instead, indiscriminately increased connectivity results in synapses between neurons that are not normally coupled. Thus, Pten loss in newborn neurons results in inappropriate excitatory synaptic connectivity.

Methods

Animals and surgeries:

All mouse procedures were performed in accordance with protocols approved by the Institutional Animal Care and Use Committee at the respective institutions. Mice were B6.129S4-Pten<tm1/hwu>/J (Pten$^{flx/flx}$; Cat# 006440) or C57Bl/6J (WT; Cat# 000664) of both sexes. 7-day-old mice were used for all experiments except for the rabies virus tracing, for which 4-week-old mice were used. Stereotaxic coordinates are presented in Supplementary Table 1. Viruses were diluted in sterile phosphate-buffered saline (PBS) to the titers listed in Supplementary Table 2.

Viruses:

pRubi, pRubi-G-T2A-Cre, and pRubi-C-T2A-Cre have been previously described (20) and were packaged using previously published methods (25). The production and application of RV-GFP/Cre-TVA-Rgp and RbV-EnvA-mCherry have also been previously described (27). For this study, the retroviral vector was modified to delete Pten in newborn neurons by replacing the nucleus-localized GFP in RV-SYN-GTRgp (27) with a GFP-Cre fusion protein. AAV-syn-mCherry-Cre, AAV-syn-Chrimson-tdT, and AAV-syn-Chronos-GFP were obtained from the University of North Carolina Vector Core. AAV-syn-Cre was obtained from University of Pennsylvania Vector Core. AAV-syn-tdT-T2A-G-Vamp2 was created by

using PCR to clone the GFP-Vamp2 fragment out of pEGFP-Vamp2 (Addgene #42308), a gift from Dr. Thierry Galli (28), with PCR primers that contained EcoR1 sites in the overhangs (forward: GAATTCGTGAGCAAGGGCGAGG; reverse: GAATTCCCTTTTAAGAGCTGAAGTAAACTATGATG), and ligating it into FUG-T2A-Cre (20). The fragment containing T2A-GFP-Vamp2 was then isolated by restriction digest and ligated into the backbone of AAV-syn-tdT-GirK2 (29), a gift from Dr. Chris Ford, using the BsrGI and HindIII sites to create AAV-syn-tdT-T2A-G-Vamp2.

To package AAV-syn-tdT-T2A-G-Vamp2 as an AAV9, we co-transfected HEK293FT cells with the serotype-specific plasmid pXR9 and the helper plasmid PADHelper, obtained from Dr. Eric Washburn, using the calcium phosphate method. After 72 hours, cells were collected in PBS, pelleted, and resuspended in a buffer containing 150mM sodium chloride and 50mM Tris, pH 8.5. Cells were lysed by freeze-thaw cycles and centrifuged to clear cell debris. The supernatant was treated with benzonase and filtered. Viral particles were isolated by density gradient centrifugation in an iodixanol gradient. The collected suspension was then diluted 50× in PBS, filtered, and reconcentrated by filter centrifugation. The prep was titered using quantitative real-time PCR with previously validated probes targeting GFP (30).

Histology, imaging, and analysis:

Histology was performed as previously described (31). Antibodies and the concentrations at which they were used are listed in Supplementary Table 3. Imaging and analysis of somata, dendritic arborization, and dendritic spines have been previously described (32). Images of axons were acquired using an LSM 810 or LSM 880 (Zeiss, Oberkochen, Germany) laser scanning confocal microscope in airyscan mode with a 63× objective, at a resolution of 1024×1024 pixels, with a 0.2μm z-step.

Electrophysiology:

Electrophysiology was performed using previously described methods (25). Animals anesthetized with tribromoethanol were transcardially perfused with chilled solution containing (in mM): 110 choline-Cl, 10 dextrose, 7 $MgCl_2$, 2.5 KCl, 1.25 NaH_2PO_4, 0.5 $CaCl_2$, 1.3 Na-ascorbate, and 25 $NaHCO_3$ and bubbled with 95% O_2-5% CO_2. Slices were held and recorded artificial cerebrospinal fluid containing (in mM): 125 $NaCl_2$, 25 $NaHCO_3$, 1.25 NaH_2PO_4, 2.5 KCl, 25 dextrose, 2 $CaCl_2$, and 1 $MgCl_2$. Recordings were performed at 37°C using intracellular solution containing (in mM): 115 K-gluconate, 10 HEPES, 2 EGTA, 20 KCl, 2 Mg-ATP, 10 Na-phosphocreatine, 0.3 Na_3-GTP. Recording pipettes had a tip resistance of 4–6MΩ. Cells were held at −90mV. Series resistance was continuously monitored, and recordings were discarded if >30% change was observed. Currents were sampled at 80kHz and filtered at 10 kHz (Multiclamp 700B, Molecular Devices, San Jose, CA, USA). mEPSCs were recorded with 1μM tetrodotoxin (R&D Systems, Minneapolis, MN, USA) in the bath. To detect mEPSCs, recordings were filtered at 2kHz, and events were automatically detected using a template with a 1ms rise, 6ms decay, and threshold of 3 (Axograph X, Axograph), then manually screened to remove false positives. Light-evoked EPSCs were recorded with 10μM SR95531 (Cayman, Ann Arbor, MI, USA) in the bath. Optogenetic stimulation was a 5ms pulse of widefield epifluorescence delivered through the

objective. A BP 470/40 filter was used for Chronos stimulation, a BP 565/30 filter for green light, and a BP 615/50 for Chrimson stimulation.

Statistical analysis:

Sample sizes are based on similar previously published experiments. No formal randomization was used to assign animals to treatment groups. In experiments with control and treatment mice, litters were split evenly between groups. Investigators were not blinded. For experiments in which each observation is a single neuron, data were analyzed using a multilevel mixed-effects linear regression model in STATA 13 (Statacorp) with post-hoc Scheffe-corrected multiple comparisons (31, 33) to take into account the nested design. All other statistical comparisons were performed in Prism (Graphpad Software). When each observation was an animal, data were analyzed using two-tailed unpaired t-tests (Figure 3, S3, S4) or Mann-Whitney tests (Figure 2E). Distributions were compared using the Kolmogorov-Smirnov test. Assumptions of normality and equal variance between groups were not tested.

Results

Sparse Pten Knockout Causes Increased Spine Density Compared to Dense Pten Knockout

We first measured the dendritic spine density of retrovirally labeled wild-type (WT) and Pten knockout neurons integrating into the early postnatal dentate gyrus. WT and Pten knockout neurons were labeled and birth-dated using control (pRubi) and Cre-expressing (pRubiG-T2A-Cre) retroviruses injected into the dentate gyrus of early postnatal (P7) $Pten^{flx/flx}$ mice (Figure 1A–D) and examined at 24 DPI. Pten knockout neurons had a higher density of dendritic spines than WT neurons (Figure 1E; z=3.69, p=0.003). In this experiment, the Pten knockout neurons developed in an environment surrounded by wild-type granule neurons. To determine if this effect persisted when Pten knockout neurons developed surrounded by other Pten knockout neurons, we repeated this experiment with Pten knocked out in the majority of surrounding neurons by injection of a high-titer Cre-expressing AAV (AAV-syn-mCherry-Cre; Figure 1A–C). This caused neuron-specific Pten knockout in mature granule neurons, as well as other neurons in the molecular layer and hilus (Figure 1C). By immunostaining for NeuN and mCherry, we found that 69.65±5.66% of NeuN-positive nuclei expressed mCherry-Cre (Figure 1C). In the dense knockout environment, the spine density of Pten knockout neurons remained higher than that of WT neurons (Figure 1E; z=9.09, p=0.000). However, Pten knockout neurons in the dense knockout environment had lower spine density than Pten knockout neurons in the WT environment (z=−3.90, p=0.002). WT neurons showed no difference in spine density between the two environments (z=−1.13, p=0.737). The interaction between Pten knockout and environment trended toward significance (z=−1.85, p=0.064).

To determine whether the decreased spine density of Pten knockout neurons in a dense Pten knockout environment resulted in a corresponding decrease in synaptic input, we recorded mEPSCs from retrovirally labeled WT and Pten knockout neurons in the WT and dense knockout environments (Figure S1). Pten knockout neurons had higher mEPSC frequency

than WT neurons in the WT environment (z=3.31, p=0.012), but not in the dense knockout environment (z=2.12, p=0.214).

Finally, we investigated whether other neuronal phenotypes associated with Pten loss were affected by the density of Pten deletion. Retrovirally-mediated Pten knockout in granule neurons causes somatic hypertrophy (20, 25, 32, 34), increased number of primary (branching directly from the soma) dendrites (20), and increased migration distance from the subgranular zone (34). Somatic hypertrophy and the number of primary dendrites were unaffected by knockout density (Figure S2D–E), and Pten knockout neurons migrated farther into the granule cell layer than WT neurons in both knockout densities (Figure S2F). Intrinsic membrane properties were also unaffected by knockout density (Figure S1C). In the dense knockout, basal dendrites, a morphological consequence of epileptiform activity, were observed on 1.1% of control neurons (1 of 85) and 44.7% of Pten knockout neurons (17 of 38; Figure S2A–C). In the WT environment, no basal dendrites were observed.

Presynaptic Bouton Density Is Not Altered by Dense Postsynaptic Pten Knockout

We next tested whether the size of the presynaptic pool is altered by dense postsynaptic Pten knockout. In order to examine the morphology of afferent axons, we developed a virus, AAV-syn-tdT-T2A-G-Vamp2, to label the axons and boutons of perforant path axons with distinct fluorophores (Figure 2A). We injected AAV-syn-tdT-T2A-G-Vamp2 into the entorhinal cortex of $Pten^{flx/flx}$ mice and either saline or AAV8-syn-Cre into the dentate gyrus (Figure 2B). Dense Pten knockout in the dentate gyrus was confirmed by immunostaining for NeuN and Pten; 83.9% (range 56.26% to 96.73%) of neurons in the granule cell layer were Pten-negative. Axons were imaged using Airyscan super-resolution microscopy at 24 DPI.

Dense postsynaptic Pten knockout did not change the frequency of axon branching within the molecular layer of the dentate gyrus (Figure 2D; t=1.729, p=0.1426). There was no change in tortuosity of axons (Figure 2E; z=−0.67, p=0.502) or in the density of GFP puncta along axon segments (Figure 2F; z=1.07, p=0.283). The average diameter of GFP puncta was no different between the environments (Figure 2G; z=1.56, p=0.086). However, axons innervating the Pten knockout environment had an altered distribution of puncta diameters, with a higher proportion of large puncta (>0.8μm) and a decreased proportion of smaller puncta (~0.4μm; Figure 2H; Kolmogorov-Smirnov test, D=0.1554, p=0.0001).

Pten Knockout Neurons Have More Presynaptic Partners

To determine whether the increased spine density conferred by Pten loss results in connectivity with an increased number of presynaptic partners, we used rabies virus (RbV)-mediated monosynaptic retrograde tracing to map neuronal connectivity of Pten knockout neurons (27). Starter cells were specified with a retrovirus (RV-GFP/Cre-TVA-Rgp) injected into the dentate gyrus of 4-week-old $Pten^{flx/flx}$ or WT mice. After 7 weeks, we injected EnvA-pseudotyped, G-deleted rabies (RbV-EnvA-mCherry) into the dentate gyrus. Connectivity was analyzed 1 week after RbV injection (Figure 3A). Pten knockout neurons showed increased neuronal connectivity with presynaptic input neurons (Figure 3B; t(8)=4.88, p=0.001). An increased number of mCherry-positive input neurons was found in

the hippocampus (t(8)=6.69, p=0.000), entorhinal cortex (t(8)=3.57, p=0.0073), and forebrain (t(8)=5.41, p=0.001). A similar number of input neurons were found in the midbrain (t(8)=1.56, p=0.157; Figure 3C).

Within the hippocampus, WT newborn neurons made direct connections with input neurons in CA1, CA3, the hilus, and the DG (Figure S3). Pten knockout neurons showed increased connectivity with DG neurons (t(8)=4.01, p=0.004), presumably due to the abnormal development of basal dendrites (26). Within the entorhinal cortex, presynaptic neurons were found in both the medial and lateral areas (Figure 3C, S3). Increased connectivity with Pten knockout neurons was observed in both entorhinal areas, specifically with the caudomedial (t(8)=3.57, p=0.0073) and dorsolateral (t(8)=3.53, p=0.008) EC, located in the medial and lateral EC, respectively. No changes were observed in the medial (t(8)=1.89, p=0.095), dorsal intermediate (t(8)=0.981, p=0.355), and ventral intermediate entorhinal fields (Figure S3). Input neurons were also found in the medial septum (MS) and horizontal nucleus of the diagonal band of Broca (HDB) in the basal forebrain, and the ventral tegmental area (VTA) and dorsal raphe nucleus (DRN) of the midbrain (Figure 3C, S3). In both forebrain areas, the connectivity ratio of Pten knockout neurons was increased (MS: t(8)=2.83, p=0.022; HDB: t(8)=3.90, p=0.005). There was no change in connectivity ratios from either subregion of the midbrain (VTA: t(8)=1.43, p=0.187; DRN: t(8)=1.55, p=0.160). DG newborn neurons also received direct inputs from commissural neurons located in the contralateral hilus (Figure 3D), the majority of which were Calretinin-positive mossy cells. Interestingly, the connectivity ratio of Pten knockout neurons with commissural mossy cells increased, indicating the convergence of mossy cell inputs from the contralateral hilus to Pten knockout neurons (t(8)=3.11, p=0.015). Finally, in animals with Pten knockout starter cells, we observed a small number of ectopic afferents arising from the thalamus (Figure S4).

Arborization and Dendritic Spines on Pten Knockout Neurons Are Increased in All Molecular Layer Subfields

The populations of glutamatergic axons innervating the DG are spatially distributed such that the lateral entorhinal area, medial entorhinal area, and mossy cells respectively innervate the outer, middle, and inner thirds of the molecular layer (35). Therefore, to determine whether Pten knockout is likely to change the frequency with which postsynaptic dendrites encounter axons from various populations, we tested whether Pten knockout altered the topographical distribution of the dendritic arbor. Retrovirally labeled WT and Pten knockout neurons were analyzed at 16DPI (Figure 4A–B). Pten knockout neurons had a longer dendritic arbor (Figure 4C, z=−12.17, p=0.000) and an increased number of primary dendrites (Figure 4D, z=2.14, p=0.032). The shape of the arbor as measured by Sholl analysis was significantly altered by Pten KO, with most increased branching proximal to the soma (Figure 4E; 2-way ANOVA, F(1,42)=31.83, p=0.0001).

To determine whether the arbor or Pten knockout neurons was distributed differently than that of WT neurons, we measured the proportion of dendritic arbor falling within each three bins of equal width defining the inner, middle, and outer thirds of the molecular layer (IML, MML, OML respectively). Pten knockout neurons did not differ from WT neurons in the

distribution of their arbor (Figure 4F; IML z=1.49, p=0.136; MML z=−0.85, p=0.398; OML z=−1.83, p=0.068).

To determine whether Pten knockout altered the distribution of dendritic spines within the dendritic arbor, we measured the density of dendritic protrusions along segments of a single dendrite as it passed through each third of the molecular layer (Figure 4G). Pten knockout increased spine density in all three subdivisions of the molecular layer (IML z=6.94, p=0.000; MML z=39.68, p=0.000; OML z=19.76, p=0.000). Both WT and Pten knockout neurons had a lower density of dendritic protrusions in the IML than in the MML and OML (comparisons not shown on graph; WT MML vs. IML z=7.46, p=0.000; WT OML vs. IML z =8.73, p=0.000; Pten KO MML vs. IML z=3.80, p=0.013; Pten KO OML vs. IML z=4.15, p=0.004). In both WT and Pten knockout neurons, protrusion density did not differ between the MML and OML (WT z=2.84, p=0.152; Pten KO z=2.13, p=0.447).

To determine whether Pten knockout altered the ratio of dendritic spines innervated by the perforant and commissural/associational paths, we determined the ratio of spine density in the outer two thirds to spine density in the inner third of the molecular layer (Figure 4I). Pten knockout did not significantly alter this ratio (z=−1.55, p=0.122). The distribution of mushroom spines (defined as protrusions having a head diameter of ≥0.18μm and a head/neck diameter ratio of ≥1.1) within the arbor mirrored the distribution of total dendritic protrusions (Figure 4J). Pten knockout significantly increased the density of mushroom-like protrusions in the IML (z=4.65, p=0.001) and MML (z=9.94, p=0.000), but not in the OML (z=2.92, p=0.130).

Pten Knockout Neurons Have Increased Input from Multiple Presynaptic Populations

The morphological and rabies-virus data suggest that Pten knockout neurons recruit increased synaptic input from all glutamatergic afferents without bias. To test this directly, we used the independently excitable opsins Chrimson and Chronos (36) to compare evoked currents from different afferents synapsing onto a single postsynaptic neuron. We injected AAV-syn-Chronos-GFP into the entorhinal cortex to express Chronos in perforant path axons, and AAV-syn-Chrimson-tdTomato into the contralateral dentate gyrus to express Chrimson in commissural axons (Figure 5A–B). At 16–18 days post-injection, we recorded light-evoked postsynaptic excitatory (leEPSC) currents from retrovirally labeled immature WT and Pten knockout neurons. In addition, we recorded from unlabeled mature WT neurons; to account for slice-to-slice variability in the number of axons infected with each virus, leEPSC amplitudes from retrovirally labeled neurons were normalized to the average of at least 2 nearby WT mature neurons.

Compared to mature neurons, 16–18-day-old (immature) WT neurons had a similar leEPSC amplitude from commissural path stimulation (z=−0.75, p=0.453), and a smaller amplitude from perforant path stimulation (Figure 6C-D, E; z=−3.39, p=0.001). Meanwhile, immature Pten knockout granule neurons compared to both mature and age-matched WT neurons had dramatically increased leEPSC amplitudes in response to both commissural (Pten KO vs. mature z=2.78, p=0.005; Pten KO vs. WT z=2.54, p=0.011) and perforant path (Pten KO vs. mature z=3.56, p=0.000; Pten KO vs. WT z=4.68, p=0.000) stimulation. Intriguingly, immature WT neurons had an increased ratio of perforant path to commissural path input

compared to mature WT neurons (Figure 5F, z=3.69, p=0.000). Pten knockout neurons had a similar ratio to mature WT neurons (z=0.12, p=0.908), but a significantly lower ratio of perforant path to commissural path input (i.e., a greater increase in commissural path input) compared to age-matched WT neurons (z=−2.21, p=0.027).

Discussion

Our results indicate that Pten knockout neurons indiscriminately recruit increased synaptic input from more presynaptic neurons than do wild-type neurons. Our system is advantageous because it allows comparison of age-matched WT and Pten knockout neurons side-by-side in the same tissue. It is important to note that while ASD patients are heterozygotes, we and others have observed concordant, but subtle increases in soma size and dendritic arborization in knockdown (25, 32) and heterozygous (37) models.

We find that newborn neurons maturing in an environment surrounded by mature Pten knockout neurons have a modest increase in spine density compared to when they are surrounded by wild-type granule neurons. We interpret this to indicate that there are a limited number of presynaptic boutons with which dendritic protrusions can stabilize, and that Pten knockout neurons are more competitive for those boutons. Alternatively, the overall synaptogenic environment of the dense knockout condition may be altered by increased network activity and involvement of inhibitory neurons. Pten deletion in >9% of granule neurons causes network hyperactivity and epilepsy (26). Though we waited only a short time after knockout, our mice were likely experiencing increased network activity as evidenced by the emergence of basal dendrites on Pten knockout neurons, which did not occur in the sparse condition. Network activity regulates the maturation of granule neurons (38), and exacerbates the overgrowth of Pten knockout neurons (24). Additionally, the dense environmental Pten knockout was not limited to granule neurons, but also included neurons in the hilus and molecular layer. In cortex, Pten deletion in interneurons causes increased IPSC frequency onto glutamatergic neurons (17). GABA release onto newborn neurons is depolarizing and regulates their maturation (39); this could contribute to the effects of network hyperexcitability on synaptic integration of the retrovirally labeled granule neurons.

We observed that presynaptic boutons enlarge, but are not created, to accommodate increased demand from postsynaptic neurons. This observation elaborates on the prevailing model of synaptogenesis in postnatally generated neurons in the dentate gyrus, which states that immature spines from newborn neurons must compete for a bouton’s synaptic territory with its preexisting postsynaptic partner (40). Our results therefore also support the model of synaptic redistribution onto newborn granule neurons (41, 42). An interesting future question is whether the enlarged boutons split to form more boutons if we were to examine later time-points after Pten deletion. The modulation of synapse number by inter-neuronal competition dynamics generalizes beyond the postnatal dentate gyrus to other brain regions since BDNF/TrkB signaling (43–45) has previously been implicated in competitive synapse formation in the cortex. Our results suggest this could be mediated by downstream AKT/mTor signaling. During development, certain synaptic cell adhesion molecules also regulate synapse number by means of inter-neuron competition for synaptic territory (46, 47), suggesting competitive synapse specification occurs throughout development. Intriguingly,

some of these effects occur through the Wnt pathway, which like the AKT/mTor pathway is a pathway of convergence for ASD risk (48).

Although we (20, 25, 32), and others (11, 22, 49) have consistently observed an increase in spine density in Pten knockout neurons *in vivo*, some studies (50, 51) have found that spine number is unaffected by Pten knockout. This discrepancy is likely explained by the density and developmental time-point of Pten deletion. Other studies showing increased spine density after Pten deletion used a sparse virally-mediated knockout (20, 22, 25, 32), or a conditional knockout that affecting only a subset of excitatory neurons (11). Studies finding no change in spine density after Pten deletion used a dense AAV injection that more closely mirrored our dense knockout (50), and a heterozygous mouse in which Pten was lost in nearly all forebrain excitatory neurons (51). Notably, both of these studies deleted Pten only in mature neurons. One conditional knockout mouse in which Pten is lost in all neurons before cellular maturation shows increased dendritic spine density (49), indicating that the effect on synapse density may be age-dependent.

Notably, of the phenotypes we evaluated, dendritic spine density was the only one attenuated by dense knockout. This is consistent with the interpretation that there is competition for a finite number of presynaptic release sites. Despite the attenuated spine density, Pten knockout neurons still recruited increased synaptic input. This is evidenced both by a similar trend toward increased mEPSC frequency in WT and competitive environments and by the presence of basal dendrites in the competitive environment, a hallmark of epileptic activity. In addition to the density of dendritic spines, a number of other factors contribute to the increased excitability of Pten knockout neurons. Pten loss can induce increased synaptic release (52), and postsynaptic mTOR activation can increase the strength of glutamatergic synapses (53). Dense virus-mediated Pten knockout in adults increases mEPSC frequency without accompanying increases in the number of synapses (50). Previously, we found that synapse number only accounted for about 27% of the increased excitatory drive onto Pten knockout neurons in sparse conditions (20). Thus, while the role of Pten in the formation and plasticity of dendritic spines remains relevant to the etiology of Pten-associated ASD, the underlying mechanism is unlikely to be solely due to increased synapse density.

Pten loss increased connectivity with a broad variety of excitatory afferents. Sparse Pten deletion was used for the rabies experiments to limit any confounds of altered network activity. All cell types with glutamatergic terminals in the dentate gyrus had increased connectivity with Pten knockout neurons, including afferents residing in the granule cell layer, hilus, and entorhinal cortex. Increased connectivity within the granule cell layer could be due to emergence of basal dendrites (26) and aberrant axon guidance (54) following Pten loss. The greatest increases in input neurons were from hilar mossy cells and the entorhinal cortex, the two primary glutamatergic projections to the dentate gyrus. Some intrahippocampal afferents, such as molecular layer interneurons, basket cells, hilar interneurons, and back-projecting interneurons from CA3, are GABAergic. We found that connectivity between Pten knockout neurons and the molecular layer, CA3, and CA1, is unchanged. These regions' only direct synapses with granule neurons are GABAergic (55). This is in accordance with our previous observations that Pten loss specifically increases

glutamatergic, but not GABAergic, input (20, 25), and suggests that Pten loss promotes synapse formation with greater numbers of all glutamatergic afferents.

Pten knockout neurons also had an increased input ratio from the medial septum and the diagonal band of Broca, which contain both GABAergic and cholinergic projections to the dentate gyrus. GABAergic projections from the septum contact primarily interneurons, whereas cholinergic projections synapse onto granule neurons (56). Previous rabies-virus tracing studies of the inputs onto granule neurons found that direct septal input to granule neurons was exclusively cholinergic (27, 57). Granule neurons express Gq-coupled M1 receptors (58). Therefore, Pten knockout neurons likely recruit additional excitatory input from cholinergic as well as glutamatergic afferents, indicating future studies on the role of acetylcholine in Pten-related models of epileptogenesis.

We confirmed the results of the rabies virus tracing with detailed morphological and physiological characterization of the enhanced connectivity of Pten knockout neurons. Arborization, spine density, and evoked synaptic currents were uniformly increased throughout the dendritic arbor, reinforcing our finding that Pten loss increases glutamatergic connectivity globally. We uniquely examined the relative contribution of two afferents to the excitatory drive of a single postsynaptic neuron. For these experiments, we did not discriminate between the lateral and medial entorhinal cortex, which differentially innervate newborn neurons (59). Intriguingly, 16–18-day-old granule neurons were highly variable and had increased input from the perforant path, despite forming their first synapses with the more proximal commissural/associational inputs (60). This could be due to the unique physiological properties of young granule neurons, in which sparse innervation and high intrinsic excitability are balanced (61, 62). By contrast, Pten knockout neurons of the same age had a balance of inputs identical to mature neurons, indicating both universally increased glutamatergic input and precocious maturation.

Our implementation of independently excitable opsins and rabies-mediated monosynaptic retrograde tracing allows for the first demonstration that the increase in synaptic input due to Pten loss is not simply an increase in the multiplicity of synapses between appropriate partners. Instead, it represents hyperconnectivity between neurons that normally would not be coupled. This inappropriate synaptic connectivity shifts the weights of synaptic inputs onto granule neurons during integration into the synaptic circuitry of the dentate gyrus. This has important implications for future studies of the role of the mTor pathway in synaptic specificity, epilepsy, pattern separation in the dentate gyrus, and the neurobiological basis of autism.

Supplementary Material

Refer to Web version on PubMed Central for supplementary material.

Acknowledgements

The work was funded by the National Institute of Mental Health (R01MH097949; to B.W.L.); and by the National Institute of Alcohol Abuse and Alcoholism (R01AA022377), the Whitehall Foundation, and the Hartwell Foundation (to H.S.).

We thank Dr. Ed Boyden for the plasmids and viruses containing Chrimson and Chronos, and for his advice on their application.

References

1. Waite KA, Eng C. Protean PTEN: Form and Function. The American Journal of Human Genetics. 2002;70(4):829–44. [PubMed: 11875759]
2. Hobert JA, Embacher R, Mester JL, Frazier TW Ii, Eng C. Biochemical screening and PTEN mutation analysis in individuals with autism spectrum disorders and macrocephaly. European Journal Of Human Genetics. 2014;22:273. [PubMed: 23695273]
3. Klein S, Sharifi-Hannauer P, Martinez-Agosto JA. Macrocephaly as a Clinical Indicator of Genetic Subtypes in Autism. Autism Research. 2013;6(1):51–6. [PubMed: 23361946]
4. Marchese M, Conti V, Valvo G, Moro F, Muratori F, Tancredi R, et al. Autism-epilepsy phenotype with macrocephaly suggests PTEN, but not GLIALCAM, genetic screening. BMC Medical Genetics. 2014;15(1):26. [PubMed: 24580998]
5. Conti S, Condò M, Posar A, Mari F, Resta N, Renieri A, et al. Phosphatase and Tensin Homolog (PTEN) Gene Mutations and Autism: Literature Review and a Case Report of a Patient With Cowden Syndrome, Autistic Disorder, and Epilepsy. Journal of Child Neurology. 2011;27(3):392–7. [PubMed: 21960672]
6. O'Roak BJ, Vives L, Fu W, Egertson JD, Stanaway IB, Phelps IG, et al. Multiplex Targeted Sequencing Identifies Recurrently Mutated Genes in Autism Spectrum Disorders. Science. 2012;338(6114):1619. [PubMed: 23160955]
7. De Rubeis S, He X, Goldberg AP, Poultney CS, Samocha K, Ercument Cicek A, et al. Synaptic, transcriptional and chromatin genes disrupted in autism. Nature. 2014;515:209. [PubMed: 25363760]
8. Stessman HAF, Xiong B, Coe BP, Wang T, Hoekzema K, Fenckova M, et al. Targeted sequencing identifies 91 neurodevelopmental-disorder risk genes with autism and developmental-disability biases. Nature genetics. 2017;49:515. [PubMed: 28191889]
9. O'Roak BJ, Vives L, Girirajan S, Karakoc E, Krumm N, Coe BP, et al. Sporadic autism exomes reveal a highly interconnected protein network of de novo mutations. Nature. 2012;485:246. [PubMed: 22495309]
10. Backman SA, Stambolic V, Suzuki A, Haight J, Elia A, Pretorius J, et al. Deletion of Pten in mouse brain causes seizures, ataxia and defects in soma size resembling Lhermitte-Duclos disease. Nature genetics. 2001;29(4):396–403. Epub 2001/12/01. [PubMed: 11726926]
11. Kwon CH, Luikart BW, Powell CM, Zhou J, Matheny SA, Zhang W, et al. Pten regulates neuronal arborization and social interaction in mice. Neuron. 2006;50(3):377–88. Epub 2006/05/06. [PubMed: 16675393]
12. Ogawa S, Kwon CH, Zhou J, Koovakkattu D, Parada LF, Sinton CM. A seizure-prone phenotype is associated with altered free-running rhythm in *Pten* mutant mice. Brain research. 2007;1168:112–23. Epub 2007/08/21. [PubMed: 17706614]
13. Clipperton-Allen AE, Page DT. Pten haploinsufficient mice show broad brain overgrowth but selective impairments in autism-relevant behavioral tests. Human Molecular Genetics. 2014;23(13):3490–505. [PubMed: 24497577]
14. Tilot AK, Gaugler MK, Yu Q, Romigh T, Yu W, Miller RH, et al. Germline disruption of Pten localization causes enhanced sex-dependent social motivation and increased glial production. Human Molecular Genetics. 2014;23(12):3212–27. [PubMed: 24470394]
15. Amiri A, Cho W, Zhou J, Birnbaum SG, Sinton CM, McKay RM, et al. *Pten* Deletion in Adult Hippocampal Neural Stem/Progenitor Cells Causes Cellular Abnormalities and Alters Neurogenesis. The Journal of Neuroscience. 2012;32(17):5880. [PubMed: 22539849]
16. Chen Y, Huang W-C, Séjourné J, Clipperton-Allen AE, Page DT. Pten Mutations Alter Brain Growth Trajectory and Allocation of Cell Types through Elevated β-Catenin Signaling. The Journal of Neuroscience. 2015;35(28):10252–67. [PubMed: 26180201]

17. Vogt D, Cho KKA, Lee AT, Sohal VS, Rubenstein JLR. The Parvalbumin/Somatostatin Ratio Is Increased in Pten Mutant Mice and by Human PTEN ASD Alleles. Cell Reports. 2015;11(6):944–56. [PubMed: 25937288]

18. Wong FK, Bercsenyi K, Sreenivasan V, Portalés A, Fernández-Otero M, Marín O. Pyramidal cell regulation of interneuron survival sculpts cortical networks. Nature. 2018;557(7707):668–73. [PubMed: 29849154]

19. Kwon CH, Zhu X, Zhang J, Knoop LL, Tharp R, Smeyne RJ, et al. Pten regulates neuronal soma size: a mouse model of Lhermitte-Duclos disease. Nature genetics. 2001;29(4):404–11. Epub 2001/12/01. [PubMed: 11726927]

20. Williams MR, DeSpenza T Jr., Li M, Gulledge AT, Luikart BW. Hyperactivity of newborn Pten knock-out neurons results from increased excitatory synaptic drive. The Journal of neuroscience : the official journal of the Society for Neuroscience. 2015;35(3):943–59. Epub 2015/01/23.

21. Diaz-Ruiz O, Zapata A, Shan L, Zhang Y, Tomac AC, Malik N, et al. Selective Deletion of PTEN in Dopamine Neurons Leads to Trophic Effects and Adaptation of Striatal Medium Spiny Projecting Neurons. PloS one. 2009;4(9):e7027. [PubMed: 19750226]

22. Xiong Q, Oviedo HV, Trotman LC, Zador AM. PTEN Regulation of Local and Long-Range Connections in Mouse Auditory Cortex. The Journal of Neuroscience. 2012;32(5):1643. [PubMed: 22302806]

23. Weston MC, Chen H, Swann JW. Multiple Roles for Mammalian Target of Rapamycin Signaling in Both Glutamatergic and GABAergic Synaptic Transmission. The Journal of Neuroscience. 2012;32(33):11441–52. [PubMed: 22895726]

24. Arafa SR, LaSarge CL, Pun RYK, Khademi S, Danzer SC. Self-reinforcing effects of mTOR hyperactive neurons on dendritic growth. Experimental Neurology. 2018.

25. Luikart BW, Schnell E, Washburn EK, Bensen AL, Tovar KR, Westbrook GL. Pten knockdown in vivo increases excitatory drive onto dentate granule cells. The Journal of neuroscience : the official journal of the Society for Neuroscience. 2011;31(11):4345–54. Epub 2011/03/18.

26. Pun Raymund YK, Rolle Isaiah J, LaSarge Candi L, Hosford Bethany E, Rosen Jules M, Uhl Juli D, et al. Excessive Activation of mTOR in Postnatally Generated Granule Cells Is Sufficient to Cause Epilepsy. Neuron. 2012;75(6):1022–34. [PubMed: 22998871]

27. Vivar C, Potter MC, Choi J, Lee J-y, Stringer TP, Callaway EM, et al. Monosynaptic inputs to new neurons in the dentate gyrus. Nature communications. 2012;3:1107.

28. Martinez-Arca S, Rudge R, Vacca M, Raposo G, Camonis J, Proux-Gillardeaux V, et al. A dual mechanism controlling the localization and function of exocytic v-SNAREs. Proceedings of the National Academy of Sciences. 2003;100(15):9011.

29. Marcott Pamela F, Mamaligas Aphroditi A, Ford Christopher P. Phasic Dopamine Release Drives Rapid Activation of Striatal D2-Receptors. Neuron. 2014;84(1):164–76. [PubMed: 25242218]

30. Fricano-Kugler CJ, Getz SA, Williams MR, Zurawel AA, DeSpenza T, Frazel PW, et al. Nuclear Excluded Autism-Associated Phosphatase and Tensin Homolog Mutations Dysregulate Neuronal Growth. Biological psychiatry. 2017.

31. Fricano CJ, Despenza T Jr., Frazel PW, Li M, O'Malley AJ, Westbrook GL, et al. Fatty acids increase neuronal hypertrophy of Pten knockdown neurons. Frontiers in molecular neuroscience. 2014;7:30 Epub 2014/05/06. [PubMed: 24795563]

32. Williams MR, Fricano-Kugler CJ, Getz SA, Skelton PD, Lee J, Rizzuto CP, et al. A Retroviral CRISPR-Cas9 System for Cellular Autism-Associated Phenotype Discovery in Developing Neurons. Scientific reports. 2016;6:25611 Epub 2016/05/11. [PubMed: 27161796]

33. Moen EL, Fricano-Kugler CJ, Luikart BW, O'Malley AJ. Analyzing Clustered Data: Why and How to Account for Multiple Observations Nested within a Study Participant? PloS one. 2016;11(1):e0146721 Epub 2016/01/15. [PubMed: 26766425]

34. Getz SA, DeSpenza T Jr., Li M, Luikart BW. Rapamycin prevents, but does not reverse, aberrant migration in Pten knockout neurons. Neurobiology of disease. 2016;93:12–20. Epub 2016/03/20. [PubMed: 26992888]

35. Witter MP, Amaral DG. CHAPTER 21 - Hippocampal Formation In: Paxinos G, editor. The Rat Nervous System (Second Edition). Second ed. Burlington: Academic Press; 1994 p. 443–83.

36. Klapoetke NC, Murata Y, Kim SS, Pulver SR, Birdsey-Benson A, Cho YK, et al. Independent optical excitation of distinct neural populations. Nature methods. 2014;11(3):338–46. Epub 2014/02/11. [PubMed: 24509633]
37. Huang W-C, Chen Y, Page DT. Hyperconnectivity of prefrontal cortex to amygdala projections in a mouse model of macrocephaly/autism syndrome. Nature communications. 2016;7:13421.
38. Piatti VC, Davies-Sala MG, Espósito MS, Mongiat LA, Trinchero MF, Schinder AF. The Timing for Neuronal Maturation in the Adult Hippocampus Is Modulated by Local Network Activity. The Journal of Neuroscience. 2011;31(21):7715. [PubMed: 21613484]
39. Dieni CV, Chancey JH, Overstreet-Wadiche LS. Dynamic functions of GABA signaling during granule cell maturation. Frontiers in neural circuits. 2012;6:113 Epub 2013/01/15. [PubMed: 23316139]
40. Toni N, Teng EM, Bushong EA, Aimone JB, Zhao C, Consiglio A, et al. Synapse formation on neurons born in the adult hippocampus. Nature neuroscience. 2007;10:727. [PubMed: 17486101]
41. McAvoy Kathleen M, Scobie Kimberly N, Berger S, Russo C, Guo N, Decharatanachart P, et al. Modulating Neuronal Competition Dynamics in the Dentate Gyrus to Rejuvenate Aging Memory Circuits. Neuron. 2016;91(6):1356–73. [PubMed: 27593178]
42. Adlaf EW, Vaden RJ, Niver AJ, Manuel AF, Onyilo VC, Araujo MT, et al. Adult-born neurons modify excitatory synaptic transmission to existing neurons. eLife. 2017;6:e19886. [PubMed: 28135190]
43. English CN, Vigers AJ, Jones KR. Genetic evidence that brain-derived neurotrophic factor mediates competitive interactions between individual cortical neurons. Proceedings of the National Academy of Sciences. 2012;109(47):19456–61.
44. Saiepour MH, Chakravarthy S, Min R, Levelt CN. Competition and Homeostasis of Excitatory and Inhibitory Connectivity in the Adult Mouse Visual Cortex. Cerebral Cortex. 2015;25(10):3713–22. [PubMed: 25316336]
45. Luikart BW, Parada LF. Receptor tyrosine kinase B-mediated excitatory synaptogenesis In: Møller AR, editor. Progress in brain research: Elsevier; 2006 p. 15–383.
46. Kwon H-B, Kozorovitskiy Y, Oh W-J, Peixoto RT, Akhtar N, Saulnier JL, et al. Neuroligin-1–dependent competition regulates cortical synaptogenesis and synapse number. Nature neuroscience. 2012;15:1667. [PubMed: 23143522]
47. Bian WJ, Miao WY, He SJ, Qiu Z, Yu X. Coordinated Spine Pruning and Maturation Mediated by Inter-Spine Competition for Cadherin/Catenin Complexes. Cell. 2015;162(4):808–22. Epub 2015/08/11. [PubMed: 26255771]
48. de la Torre-Ubieta L, Won H, Stein JL, Geschwind DH. Advancing the understanding of autism disease mechanisms through genetics. Nature Medicine. 2016;22:345.
49. Fraser MM, Bayazitov IT, Zakharenko SS, Baker SJ. Phosphatase and tensin homolog, deleted on chromosome 10 deficiency in brain causes defects in synaptic structure, transmission and plasticity, and myelination abnormalities. Neuroscience. 2008;151(2):476–88. [PubMed: 18082964]
50. Haws ME, Jaramillo TC, Espinosa F, J. Widman A, Stuber GD, Sparta DR, et al. PTEN knockdown alters dendritic spine/protrusion morphology, not density. Journal of Comparative Neurology. 2014;522(5):1171–90. [PubMed: 24264880]
51. Sperow M, Berry RB, Bayazitov IT, Zhu G, Baker SJ, Zakharenko SS. Phosphatase and tensin homologue (PTEN) regulates synaptic plasticity independently of its effect on neuronal morphology and migration. J Physiol. 2012;590(4):777–92. [PubMed: 22147265]
52. Weston M, Chen H, Swann J. Loss of mTOR repressors Tsc1 or Pten has divergent effects on excitatory and inhibitory synaptic transmission in single hippocampal neuron cultures. Frontiers in molecular neuroscience. 2014;7(1).
53. Henry FE, McCartney AJ, Neely R, Perez AS, Carruthers CJL, Stuenkel EL, et al. Retrograde Changes in Presynaptic Function Driven by Dendritic mTORC1. The Journal of Neuroscience. 2012;32(48):17128. [PubMed: 23197706]
54. LaSarge CL, Santos VR, Danzer SC. PTEN deletion from adult-generated dentate granule cells disrupts granule cell mossy fiber axon structure. Neurobiology of disease. 2015;75:142–50. [PubMed: 25600212]

55. Scharfman HE. The CA3 “backprojection” to the dentate gyrus In: Scharfman HE, editor. Progress in brain research: Elsevier; 2007 p. 627–37.

56. Leranth C, Hajszan T. Extrinsic afferent systems to the dentate gyrus In: Scharfman HE, editor. Progress in brain research: Elsevier; 2007 p. 63–799.

57. Deshpande A, Bergami M, Ghanem A, Conzelmann K-K, Lepier A, Götz M, et al. Retrograde monosynaptic tracing reveals the temporal evolution of inputs onto new neurons in the adult dentate gyrus and olfactory bulb. Proceedings of the National Academy of Sciences. 2013;110(12):E1152.

58. Martinello K, Huang Z, Lujan R, Tran B, Watanabe M, Cooper Edward C, et al. Cholinergic Afferent Stimulation Induces Axonal Function Plasticity in Adult Hippocampal Granule Cells. Neuron. 2015;85(2):346–63. [PubMed: 25578363]

59. Woods NI, Vaaga CE, Chatzi C, Adelson JD, Collie MF, Perederiy JV, et al. Preferential Targeting of Lateral Entorhinal Inputs onto Newly Integrated Granule Cells. The Journal of Neuroscience. 2018;38(26):5843–53. [PubMed: 29793975]

60. Chancey JH, Poulsen DJ, Wadiche JI, Overstreet-Wadiche L. Hilar Mossy Cells Provide the First Glutamatergic Synapses to Adult-Born Dentate Granule Cells. The Journal of Neuroscience. 2014;34(6):2349. [PubMed: 24501373]

61. Dieni CV, Nietz AK, Panichi R, Wadiche JI, Overstreet-Wadiche L. Distinct Determinants of Sparse Activation during Granule Cell Maturation. The Journal of Neuroscience. 2013;33(49): 19131. [PubMed: 24305810]

62. Dieni CV, Panichi R, Aimone JB, Kuo CT, Wadiche JI, Overstreet-Wadiche L. Low excitatory innervation balances high intrinsic excitability of immature dentate neurons. Nature communications. 2016;7:11313.

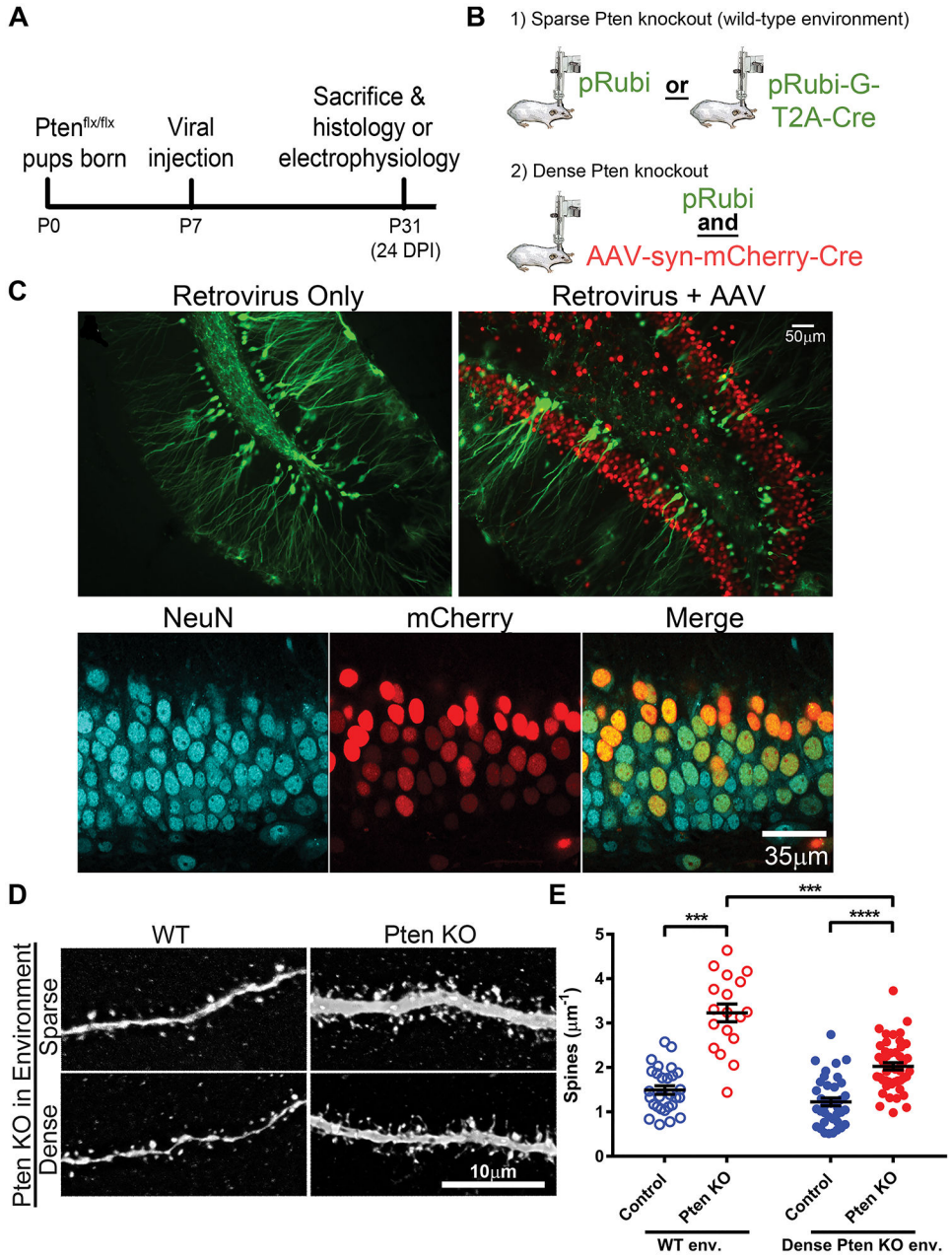

Figure 1. Pten knockout neurons have increased dendritic spine density when knockout is sparse.

(A) Virus was injected into the dentate gyrus of Pten$^{flx/flx}$ mice at postnatal day 7. Experiments were conducted at 24 days post-injection (postnatal day 31). (B) Sparse Pten knockout and labeling of newborn neurons was achieved by injection of control (pRubi) or Cre-expressing (pRubi-G-T2A-Cre) retroviruses into Pten$^{flx/flx}$ mice. Dense Pten knockout was achieved by coinjecting a control retrovirus (pRubi) and Cre-expressing AAV (AAV-syn-mCherry-Cre). (C) Example images of retrovirally labeled neurons in the sparse condition (left) and retrovirus- and AAV-infected neurons in the competitive condition (right). WT neurons expressed GFP only, while Pten knockout neurons expressed GFP and mCherry. (C, bottom) 69.65±5.66% of NeuN+ cells expressed mCherry-Cre. (D)

Representative images of WT and Pten knockout dendrites surrounded by sparse (top) or dense (bottom) Pten knockout granule neurons. (E) Pten knockout neurons have increased dendritic spine density in environments with both sparse (open circles) and dense (closed circles) Pten knockout. Pten knockout neurons in the dense Pten knockout environment have a reduced spine density compared to Pten knockout neurons in the sparse Pten knockout environment (WT sparse: n=28 neurons from 3 animals, 1.4943±0.095μm^{-1}; Pten KO sparse: n=18 neurons from 3 animals, 3.2326±0.200μm^{-1}; WT dense: 38 neurons from 5 animals, 1.2271±0.088μm^{-1}; Pten KO dense: 47 neurons from 5 animals, 2.0275±0.081μm^{-1}. Main effects: Pten KO: z=2.31, p=0.21; environment: z=0.82, p=0.410; interaction: z=−1.85, p=0.064. Pairwise comparisons: Pten KO sparse vs. WT sparse: z=3.69, p=0.003; Pten KO dense vs. WT dense: z=9.09, p=0.000; WT dense vs. WT sparse: z=−1.13, p=0.737; Pten KO dense vs. Pten KO sparse: z=−3.90, p=0.002). See also Figure S1.

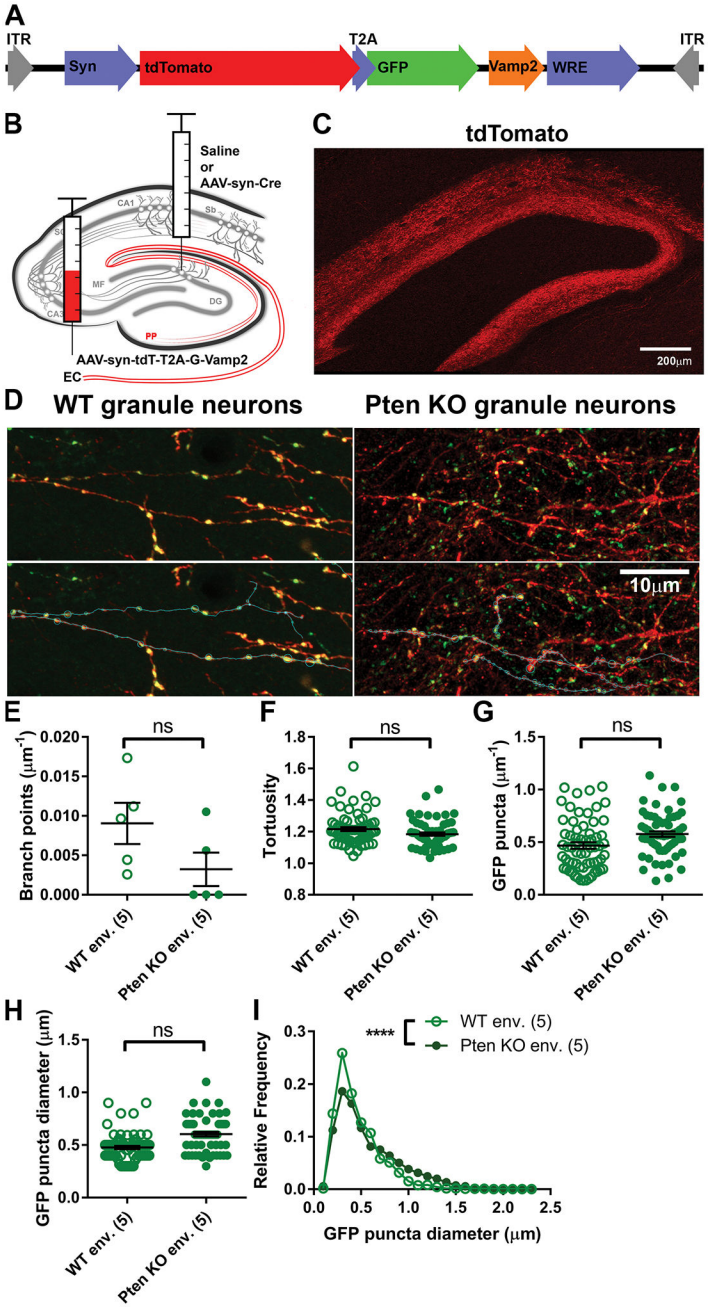

Figure 2. Dense postsynaptic Pten knockout does not alter the density of presynaptic boutons.

(A) Schematic of the AAV-syn-tdT-T2A-G-Vamp2 construct, which was packaged as an AAV9. (B) AAV-syn-tdT-T2A-G-Vamp2 was injected into the entorhinal cortex to label perforant path axons. Saline or AAV-syn-Cre was injected into the dentate gyrus for the WT or dense Pten knockout conditions, respectively. (C) Example image of tdTomato-filled axons in the dentate gyrus. (D) Example images of PP axons in the DG expressing cell-filling tdTomato and GFP localized to putative synapses. Segments of axons in the PP were traced (below), and the locations and size of GFP+ puncta, putative synaptic terminals, were recorded. (E-G) Postsynaptic Pten knockout had no effect on the frequency of axon

branching (E; n=5 mice per condition; WT env.: 0.009046±0.002615μm^{-1}, Pten KO env.: 0.003225±0.002123μm^{-1}; Welch-corrected Mann-Whitney test: t=1.729, df=7.676, p=0.1426), tortuosity of axon segments (F; WT env.: n=65 axon segments from 5 animals, WT env.: 1.216±0.125; Pten KO env.: n=62 segments from 5 animals, 1.184±0.011; z= −0.67, p=0.502), or density of GFP puncta within an axon (G; WT env.: 0.4683±0.030μm^{-1}: Pten KO env.: 0.5772±0.026μm^{-1}, z=1.07, p=0.283). (H-I) The average diameter of GFP puncta was unchanged in the dense Pten knockout postsynaptic environment (H; WT env.: 0.4767±0.017μm; Pten KO env.: 0.6037±0.021μm, z=1.72, p=0.086), but the distribution (I) was altered (KS test; WT env.: n=1460 puncta, Pten KO env.: n=1675 puncta; D=0.1554, p=0.0001). Data are presented as mean±SEM.

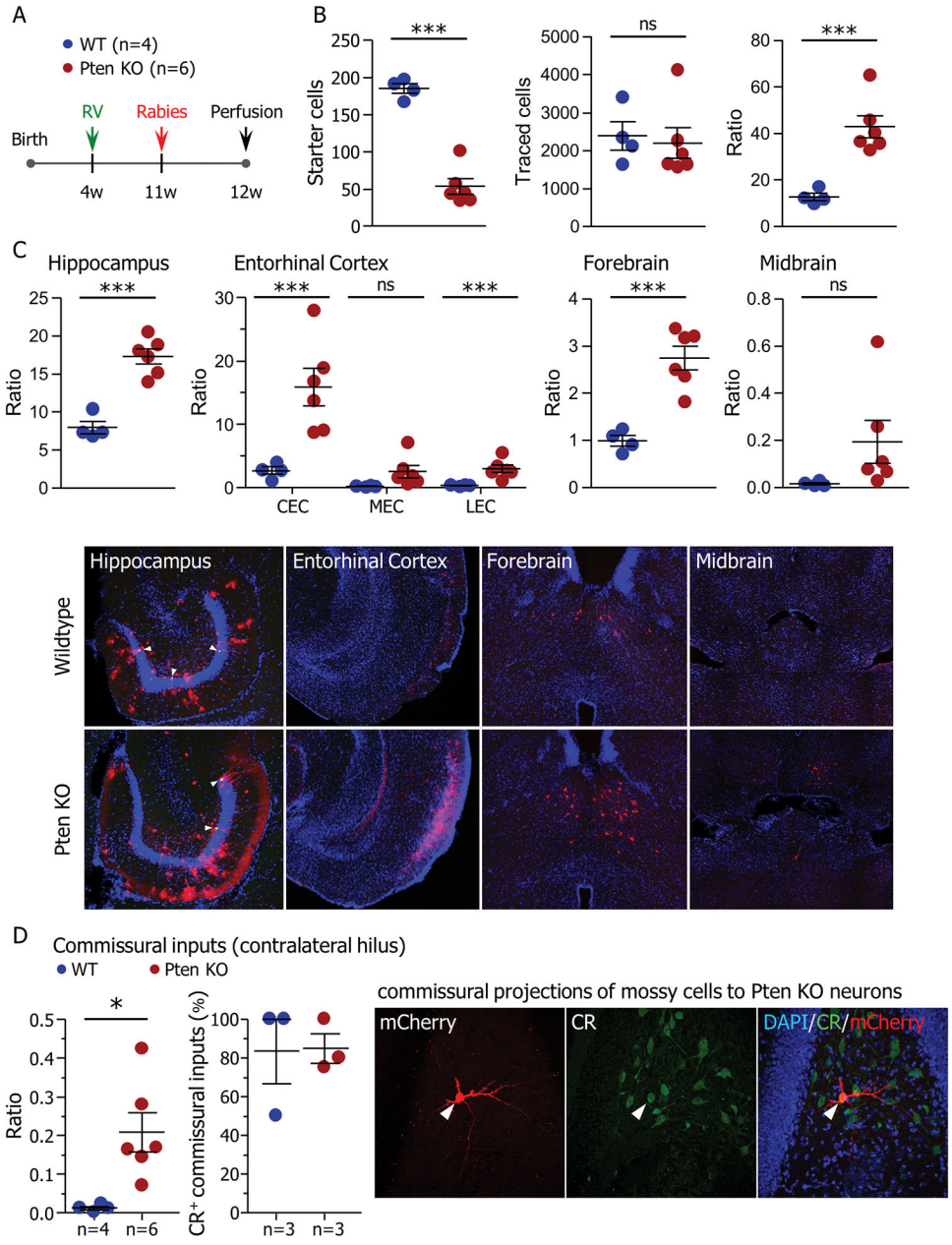

Figure 3. Pten knockout neurons have more presynaptic partners.

(A) Starter retrovirus (RV-GFP/Cre-TVA-Rgp) was injected into the dentate gyrus of 4-week-old Pten$^{flx/flx}$ or control (WT) mice. Seven weeks later, rabies virus (RbV-EnvA-mCherry) was injected at the same coordinate. Connectivity was analyzed one week after rabies virus injection and eight weeks after birth of starter neurons. (B) Quantification of starter cells positive for both retrovirus and rabies virus (left; WT: 185.3±6.524, Pten KO: 53.33 ± 10.30, t(8)=9.51, p=0.000), and total input cells (rabies virus only; middle; WT: 2389±371.2, Pten KO: 2200±399.9, t(8)=0.326, p=0.753). The ratio of input cells to starter cells (right) was higher in Pten$^{flx/flx}$ mice than in controls (WT: 12.75±1.581, Pten KO: 42.83±4.828, t(8)=4.88, p=0.001). (C; top) Region-specific connectivity ratios. Pten knockout granule neurons had higher connectivity with the hippocampus (HPC; WT:

8.005±0.8224, Pten KO: 17.33±0.9861, t(8)=6.69, p=0.000), Entorhinal cortex (EC; CEC = caudal EC: WT: 2.675±0.5888, Pten KO: 15.89±2.937, t(8)=3.57, p=0.0073; MEC = medial EC: WT: 0.2425±0.06537, Pten KO: 2.573±0.9835, t(8)=1.89, p=0.095; LEC = lateral EC: WT: 0.3525±0.06981, Pten KO: 2.970±0.5921, t(8)=3.53, p=0.008), and basal forebrain (fb; WT: 0.9975±0.1145, Pten KO: 2.748±0.2484, t(8)=5.41, p=0.001). There was no change in connectivity ratio with the midbrain (Mb; WT: 0.0175±0.004787, Pten KO: 0.1950±0.09095, t(8)=1.56, p=0.157). (C; bottom) Example images showing input neurons (mCherry) in the hippocampus, entorhinal cortex, forebrain, and midbrain. White arrowheads denote starter cells expressing both mCherry and GFP from the starter retrovirus. (D) Inputs from the contralateral hilus. Pten knockout neurons had a greater connectivity ratio with the contralateral hilus (WT: 0.0106±0.004475, Pten KO: 0.2084±0.05082, t(8)=3.11, p=0.015). The majority of inputs onto both WT and Pten knockout neurons from the contralateral hilus were positive for calretinin (CR^+; WT: n=3 animals, 83.33±16.67%, Pten KO: n=3 animals, 85.00±7.638%, t(4)=0.091, p=0.932). Data are presented as mean±SEM. Except where otherwise stated, n=4 WT animals and 6 $Pten^{flx/flx}$ animals. All tests are two-tailed unpaired t-tests. See also Figures S3 and S4.

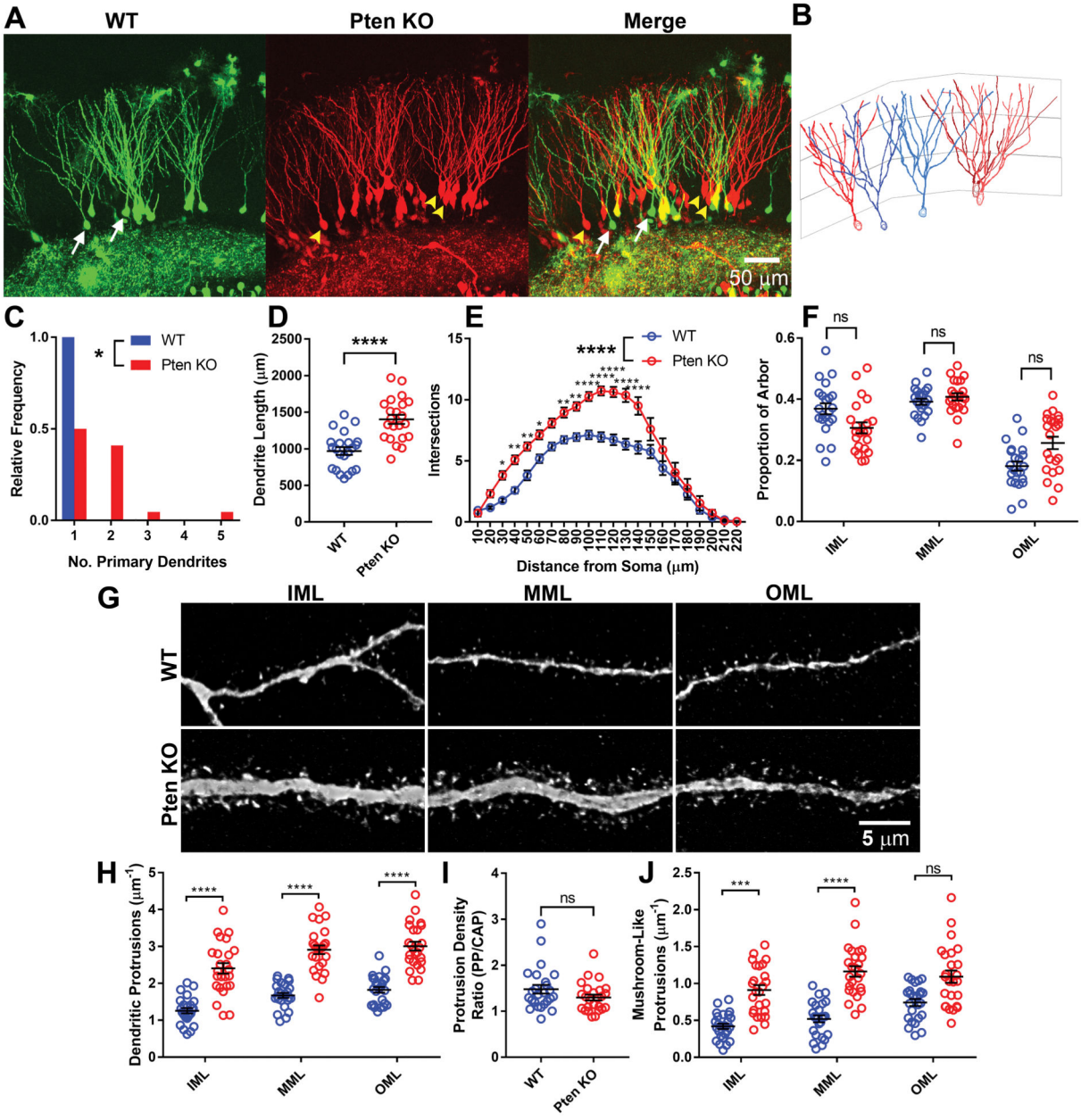

Figure 4. Pten knockout increases arborization in all molecular layer subfields

(A) Example images of retrovirally labeled 16-DPI WT (GFP) and Pten knockout (mCherry) DG granule neurons. Arrows denote neurons reconstructed in (B). (B) Reconstructions of granule neurons. WT neuron reconstructions are in blue and denoted by white arrows in (A); Pten knockout neuron reconstructions are red and denoted by yellow arrowheads. The overlaid grid denotes the boundaries approximating the inner, middle, and outer thirds of the molecular layer (IML, MML, OML, respectively). (C) Histogram of the number of primary dendrites on WT and Pten knockout neurons. All WT neurons had a single primary dendrite; 50% of Pten knockout neurons had ≥2 (n=22 WT, 22 Pten KO neurons from 5 animals; z=2.14; p=0.032). (D) The total length of the dendritic arbor was greater for Pten knockout neurons than for WT neurons (WT: 968.8±53.11μm, Pten KO: 1402±62.45μm; z=−12.17,

p=0.000). (E) Sholl analysis. Pten knockout neurons branched more throughout the dendritic arbor (2-way ANOVA with matching for intersections; F(1,42)=31.83, p=0.0001). (F) The proportion of the reconstructed arbors falling into the inner, middle, and outer thirds of the molecular layer (IML WT: 0.369±0.018, Pten KO: 0.306±0.018, z=1.49, p=0.136; MML WT: 0.392±0.010, Pten KO: 0.408±0.012, z=0.85, p=0.398; OML WT: 0.181±0.015, Pten KO: 0.257±0.020, z=−1.83, p=0.068). (G) Representative images of WT (top) and Pten knockout (bottom) neurites. Images were collected from the inner, middle, and outer thirds of the molecular layer. (H) Pten knockout neurons had a higher density of dendritic protrusions within each third of the molecular layer (n=25 WT and 25 Pten KO neurites from 5 animals; Main effects: Layer: z=2.81, p=0.005; Pten KO: z=5.35, p=0.000; interaction: z=0.22, p=0.823; post-hoc comparisons: IML WT: 1.258±0.073, Pten KO 2.406±0.143, z=6.94, p=0.000; MML WT: 1.672±0.067, Pten KO: 2.910±0.116, z=39.68, p=0.000; OML WT: 1.825±0.078, Pten KO: 3.008±0.118, z=19.76, p=0.000). Both Pten knockout and WT neurons had a significantly lower density of dendritic protrusions in the IML compared to both the MML and OML (significance not shown; WT MML vs. IML: z=7.46, p=0.000; WT OML vs. IML: z=8.73, p=0.000; Pten KO MML vs. IML: z=3.80, p=0.013; Pten KO OML vs. IML: z=4.14, p=0.004). OML did not differ from MML in either genotype (WT: z=2.84, p=0.152; Pten KO: z=2.13, p=0.477). (I) The ratio of dendritic protrusion density in areas innervated by the perforant path (PP) to dendritic protrusion density in areas innervated by the commissural/associational path (C/AP) was calculated by dividing the spine density in the MML and OML by the spine density in the IML. The ratio of PP to C/AP spine density was not changed by Pten knockout (WT: 1.179±0.094; Pten KO: 1.300±0.064; z=−1.55, p=0.122). (J) Pten knockout neurons have an increased density of mushroom-spine-like protrusions in both the IML and MML compared to WT neurons (Main effects: Layer: z=2.44, p=0.015; Pten KO: z=4.54, p=0.000; interaction: z=−0.94, p=0.347; IML WT: 0.420±0.036, Pten KO: 0.911±0.066, z=4.65, p=0.001; MML WT: 0.520±0.047, Pten KO: 1.164±0.070, z=9.94, p=0.000; OML WT: 0.743±0.048, Pten KO 1.93±0.083, z=2.92, p=0.130). All data are represented as mean±SEM.

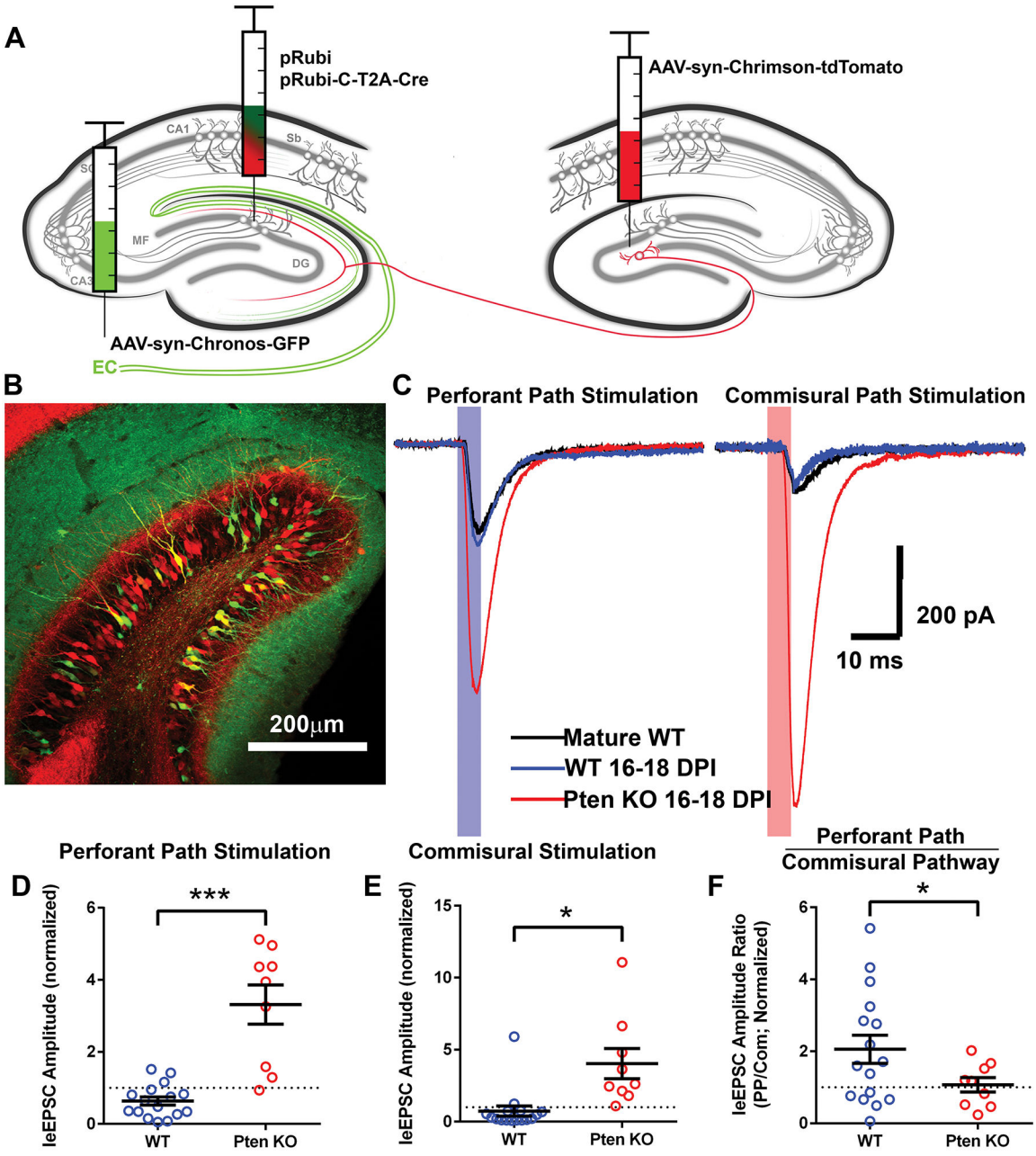

Figure 5. Pten knockout neurons recruit increased synaptic input from multiple brain regions.

(A) In 7-day-old Pten$^{flx/flx}$ mice, postnatally generated neurons in the dentate gyrus were labeled and birth-dated with control and Cre-expressing retroviruses. AAVs expressing independently excitable channelrhodopsins were injected into the entorhinal cortex and contralateral dentate gyrus. While recording from retrovirally labeled granule neurons, afferent pathways were stimulated by a 5ms pulse of blue or red light directed at the molecular layer delivered through the objective. (B) Chronos-GFP-expressing axons of the perforant path are present in the outer two-thirds of the molecular layer, and the inner molecular layer is occupied by Chrimson-tdTomato-expressing axons of the commissural pathway. Retrovirally labeled 16-day-old granule neurons are present in the granule cell

layer. (C) Example light-evoked postsynaptic currents recorded from a triad consisting of a WT mature (black), a WT immature (blue), and a Pten knockout immature (red) neuron. The shaded area represents the duration of the light pulse. (D) Perforant path stimulation evoked larger postsynaptic currents in Pten knockout neurons than in adjacent WT neurons. To control for slice-to-slice variability, values are normalized to the amplitudes of light-evoked EPSCs recorded from adjacent mature neurons (n=16 mature, 16 WT, 9 Pten KO neurons from 5 animals; WT: 0.636±0.114, Pten KO: 3.315±0.544; WT vs. mature: z=−3.39, p=0.003; Pten KO vs. mature: z=3.56, p=0.002; Pten KO vs. WT: z=4.68, p=0.000). (E) Commissural pathway stimulation evoked larger EPSCs in Pten knockout neurons than in adjacent WT neurons. To control for slice-to-slice variability, values are expressed as a factor of the light-evoked current amplitudes recorded from adjacent mature granule neurons (WT: 0.734±0.354; Pten KO: 4.032±1.046; WT vs. mature: z=−0.75, p=0.754; Pten KO vs. mature: z=2.78, p=0.021; Pten KO vs. WT: z=2.54; p=0.040). (F) Pten knockout neurons had a decreased ratio of perforant path to commissural path input compared to immature WT neurons, but a similar ratio to that of mature WT neurons (WT: 2.056±0.391; Pten KO: 1.07±0.301; WT vs. mature: z=3.69, p=0.001; Pten KO vs. mature: z=0.12, p=0.993; Pten KO vs. WT: z=−2.21, p=0.027). Data are presented as mean±SEM. EC=entorhinal cortex; leEPSC=light-evoked excitatory post-synaptic current; PP=perforant path; Com=commissural path. See also Figures S5 and S6.